Poisson-Distributed Electron-Transfer Dynamics from Single Quantum Dots to C60 Molecules

Nianhui Song,[†] Haiming Zhu,[†] Shengye Jin,[†] Wei Zhan,[‡] and Tianquan Lian[†,*]

[†]Department of Chemistry, Emory University, Atlanta, Georgia 30322, United States, and [‡]Department of Chemistry and Biochemistry, Auburn University, Auburn, Alabama 36849, United States

ABSTRACT Functional quantum dot (QD)-based nanostructures are often constructed through the self-assembly of QDs with binding partners (molecules or other nanoparticles), a process that leads to a statistical distribution of the number of binding partners. Using single QD fluorescence spectroscopy, we probe this distribution and its effect on the function (electron-transfer dynamics) in QD—C60 complexes. Ensemble-averaged transient absorption and fluorescence decay as well as single QD fluorescence decay measurements show that the QD exciton emission was quenched by electron transfer from the QD to C60 molecules and the electron-transfer rate increases with the C60-to-QD ratio. The electron-transfer rate of single QD—C60 complexes fluctuates with time and varies among different QDs. The standard deviation increases linearly with the average of electron-transfer rates of single QD—C60 complexes, and the distributions of both quantities obey Poisson statistics. The observed distributions of single QD—C60 complexes and ensemble-averaged fluorescence decay kinetics can be described by a model that assumes a Poisson distribution of the number of adsorbed C60 molecules per QD. Our findings suggest that, in self-assembled QD nanostructures, the statistical distribution of the number of adsorbed partners can dominate the distributions of the averages and standard deviation of their interfacial dynamical properties.

KEYWORDS: quantum dots · fullerene · interfacial electron transfer · single particle spectroscopy

Understanding charge- and energy-transfer dynamics in quantum dot (QD)-based nanostructures is essential to their many potential applications, such as solar cells,[1−3] light-emitting diodes,[4−6] and biological imaging and detection.[7−9] Förster resonance energy transfer in QD−molecular acceptor pairs has been extensively studied for biological sensing applications.[9−13] Interest in charge transfer from QDs to acceptors[2,14−27] has intensified in recent years due to reports of the highly controversial multiexciton generation (MEG) processes in some QDs.[28−31] Functional QD−molecule complexes (for energy or charge transfer) are often constructed by linking the molecule to a QD by either replacing or reacting with the ligands on the QD surface.[7−16,32] This process generates QDs with a distribution of adsorbed acceptors on the surface.[33] Similar heterogeneous distributions should also exist in other nanoparticle−molecule or nanoparticle−nanoparticle complexes. Thus, knowledge of the nature of this distribution is important to the understanding of the properties of QD-based nanostructures. The distribution is often assumed to be Poisson because of the discrete and small number of adsorbed molecules.[17,34] The distribution can be both static (varying among QDs) and dynamic (fluctuating with time) and is difficult to determine by ensemble-averaged techniques, such as fluorescence decay and transient absorption spectroscopy. Single particle/molecule fluorescence spectroscopy has been shown to be a powerful tool for directly probing these distributions[33,35−38] and has been used to probe the heterogeneity of electron transfer[14,39,40] and Förster resonance energy-transfer[33] dynamics in QD nanostructures.

In this paper, we report a study of electron transfer (ET) from single QDs to adsorbed fullerene C60 as a model system of QD−molecule and QD−nanoparticle complexes. C60 is a well-characterized electron acceptor, and electron transfer from CdSe QDs to C60 has been previously reported by ensemble-averaged measurements.[41−44] The monomalonic derivative of fullerene C60 (C60) molecules used in this study (shown in Figure 1a, inset) have two carboxylic groups that facilitate their binding with QDs. We probe directly the fluorescence decay of single QD−C60 complexes, from which the distribution of electron-transfer rates is obtained. We show that the ET rates vary among different single QD−C60 complexes and fluctuate with time, and the extent of the dynamic fluctuation (quantified by standard deviation) increases with the average ET rate. Both the average and the standard deviation of ET rates in single

*Address correspondence to tlian@emory.edu.

Received for review October 19, 2010 and accepted December 15, 2010.

Published online December 29, 2010.
10.1021/nn1028828

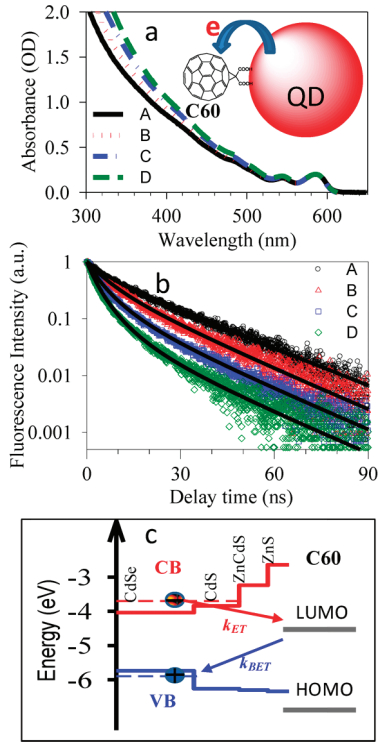

Figure 1. (a) UV−vis absorption spectra (lines) and (b) ensemble-averaged fluorescence decays (open symbols) of QD−C60 complexes from samples A (black, free QDs), B (red), C (blue), and D (green). The inset of (a) shows a scheme of a 1:1 QD−C60 complex. Solid lines in (b) are best fits according to the Poisson distribution model described in the main text. (c) Energetic diagram of the QD−C60 complex and possible charge-transfer processes: ET from the QD conduction band (CB) to C60 LUMO, followed by the back ET process.

QD−C60 complexes obey the Poisson distribution. We propose a model to account for these distributions, which is shown to be caused by the Poisson statistics of the number of adsorbed C60 on QDs in these self-assembled nanostructures.

RESULTS AND DISCUSSION

Ensemble-Averaged Fluorescence Decay. The UV−vis spectra of samples A, B, C, and D (QD−C60 water solution) used for the ensemble-averaged studies are displayed in Figure 1a. These spectra show the same first exciton peak absorption at 585 nm for the water-soluble CdSe/$CdS_{2\ ML}$/$CdZnS_{1\ ML}$/$ZnS_{1\ ML}$ core/shell QDs, as well as increased C60 absorption (broad feature at <500 nm) from sample A to sample D, indicating a constant QD concentration and increasing C60-to-QD ratio from sample A (free QD without C60) to sample D. The exact adsorbed C60-to-QD ratios are not determined because the extinction coefficient of the QD is not known and there are some free C60 molecules in water due to the non-negligible solubility of C60 in water. Ensemble-averaged fluorescence decays of these samples are shown in Figure 1b. The measurement was carried out under the same conditions as the single QD fluorescence study (except for the lower concentration of QD−C60 complexes). For both measurements, the solutions were spin-coated on thin glass coverslips and dried in air. The QD fluorescence from 540 to 625 nm was collected after the excitation of the sample at 500 nm. It is clear from Figure 1b that a faster exciton decay was observed in QD−C60 complexes compared with the free QDs and the exciton quenching rate increases with the C60-to-QD ratio.

Possible reasons for the observed exciton quenching in QD−C60 complexes are discussed based on the relative positions of the conduction band (CB) and valence band (VB) in the QD and the highest occupied molecular orbital (HOMO) and lowest unoccupied molecular orbital (LUMO) of C60, as shown in Figure 1c. From the first exciton peak position of the QDs, the conduction and valence band levels can be estimated to be −3.84 and −5.77 V (relative to vacuum) according to the method reported in previous studies.[45−47] These values are consistent with measured ones for CdSe core only QDs of similar sizes.[48,49] The LUMO and HOMO levels of C60 molecules were reported to be −4.30 and −6.60 V, respectively.[50,51] Hole transfer from QDs to C60 is energetically forbidden in this system. Energy transfer is not possible, either, because of the lack of spectral overlap of the QD emission with C60 absorption. Electron transfer from the QD conduction band to the LUMO of C60 is energetically allowed and has been reported in previous works.[41−44]

To provide further evidence of the ET pathway, we also carried out a transient absorption study of the QD−C60 complexes. As shown in Figures S1 and S2 (Supporting Information), in the presence of C60, the QD 1s exciton bleach shows a faster recovery on the nanosecond time scale than the free QDs. The bleach of the 1s exciton absorption results from the filling of the 1s level in the conduction band by the excited electron, and its recovery indicates the removal of the 1s electron.[15−17,34,52,53] Faster bleach recovery in the QD−C60 complexes suggests an additional decay pathway for the 1s electron: by electron transfer to the C60 molecules. We have previously shown that the kinetics of QD exciton bleach recovery agrees with the formation of reduced adsorbates, confirming the assignment of the exciton bleach recovery to the interfacial ET process.[15,16,34,53] Unfortunately, the absorption band of reduced C60 molecules falls in the near IR, beyond the spectral window of our current setup. We also showed previously that the transfer of holes from QDs to adsorbates does not lead to the recovery of the 1s exciton bleach.[17] Together, the results of fluorescence decay and transient absorption suggest that exciton quenching in the QD−C60 complexes can be attributed to the electron transfer from excited QDs to adsorbed C60 molecules.

ET Dynamics in Single QD−C60 Complexes. Single QD fluorescence detection was carried out with a home-built scanning confocal microscope. A raster scan fluores-

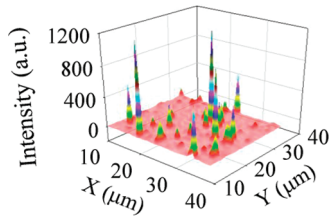

Figure 2. Raster scan fluorescence image of single QD−C60 complexes on a glass coverslip.

cence image of single QD−C60 complexes is shown in Figure 2, indicating spatially well-separated single particles.

Four samples of QD−C60 complexes are compared in this study. The C60-to-QD ratios increase from sample 1 (free QD) to sample 4, although the exact ratio was not accurately determined due to the inability to record accurate absorption spectra under such a low concentration (~10 pM) of QDs. Fifty single QDs from each sample were detected and examined, and each QD was followed for about 5 min. No noticeable permanent photobleach was observed in this time duration. For each detected photon, both the delay time (relative to the excitation pulse) and the arrival time (relative to the start of experiment) were recorded. For each QD, photons within 50 ms arrival time windows were binned to construct the intensity trajectory. The delay time histograms of photons within 2 s arrival time windows were constructed and fitted to single exponential decay functions (by nonlinear least-squares fit) to obtain the lifetime or decay rate (inverse of lifetime) trajectory. Typical intensity and lifetime trajectories of single QD and QD−C60 complexes from these samples are shown in panels a1−a4 in Figure 3. The lifetime trajectory follows the intensity trajectory for both free QDs and QD−C60 complexes, consistent with the reported positive correlation between the fluorescence intensity and lifetime of single QDs.[14,39,47,54−65] States with higher fluorescence intensity (on-state) have longer exciton lifetimes, and states of low intensity (off-state) have shorter lifetimes. The off-states have been attributed to charged QDs, formed by photoinduced Auger ionization and/or charge transfer to trap states.[35,55−57,59,65−67] We attribute all points with intensity within three standard deviations of the background level to off-states and all points with higher intensities to on-states. The exciton decay rate distributions for the single QDs shown in panels a1−a4 are plotted in panels b1−b4 (Figure 3). The green bar in each histogram indicates the occurrence of off-states with decay rates larger than 2 ns^{-1} (or lifetimes < 0.5 ns). The decay rates at these points cannot be accurately determined because of limited photon numbers.

Similar fluorescence decay rate distributions were found in other single QDs and QD−C60 complexes. To represent the rate distribution of the ensemble of single QD−C60 complexes in each sample, total histograms of exciton decay rate distributions were constructed from the sum of 50 single QD−C60 rate histograms and are shown in Figure 3c1−c4. In the absence of adsorbed electron acceptors, single free QDs (Figure 3b1,c1) already show a fluctuation of exciton decay rates, from ~0.03 ns^{-1} in the on-state to >0.5 ns^{-1} in the off-state. The QD on-state decay rate shifts from 0.1 to 0.6 ns^{-1} in samples 2−4, increasing with the average C60-to-QD ratios. The contributions of off-state increase in these samples, although their decay rates remain too fast to be measured. A similar behavior was also observed in a previous study of ET from single QDs to TiO_2, in which it was shown that the presence of the

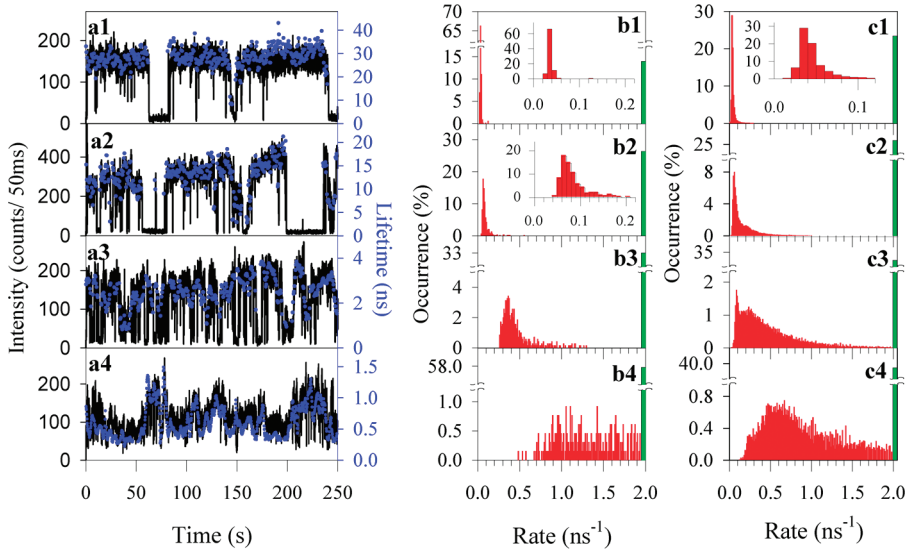

Figure 3. Typical fluorescence intensity (black line) and lifetime (blue circles) trajectories (a*i*) and histograms of the exciton quenching rate (with a 0.01 ns^{-1} bin) (b*i*) of a representative single QD or QD−C60 complex from each sample (*i* = 1−4 for samples 1−4, respectively). (c*i*) Total histogram of exciton quenching rates constructed from 50 particles in each sample. Green bars in (b*i*) and (c*i*) indicate the occurrence of low fluorescence intensity points along the trajectories, for which the rates have been assumed to be >2 ns^{-1}.

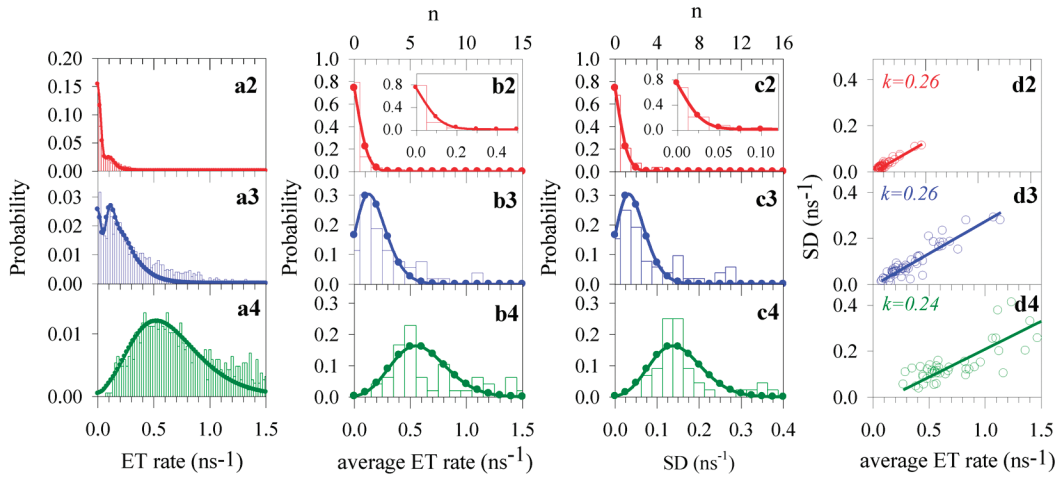

Figure 4. Histograms of ET rates (a*i*), average ET rates (b*i*), and standard deviations of ET rates (c*i*) and plots of standard deviations *vs* average ET rates (d*i*) for QD−C60 complexes from samples *i* (=2, 3, 4). Bars are experimental data, and solid lines are fits to Poisson distributions according to the model described in the text. Insets in panels b2 and c2 show an expanded view at the region of low ET rates and standard deviation. The histograms in (b*i*) and (c*i*) were constructed using bin sizes that are equal to the average ET rate k_1 (0.10 ns^{-1}) and standard deviation SD_1 (0.025 ns^{-1}), respectively, of the 1:1 C60−QD complex. The number of C60 (*n*) corresponding to the average ET rate and standard deviation is labeled as the top horizontal axes of panels b2 and c2.

ET pathway increases the probability density of long off-states.[39] The exciton decay rate of free QDs contains the contribution of the intrinsic radiative and nonradiative decay processes. For C60−QD complexes, the presence of the ET process adds an additional nonradiative pathway and increases the exciton decay rate. However, the fluctuation of exciton decay rates in free QDs complicates the determination of ET rates from the measured total exciton decay rates in single QD−C60 complexes. This complication can be removed by considering the dynamics in the on- and off-states separately. It was shown previously that, for single QDs on TiO_2, the off-state decay rate was much faster than the ET rate and was dominated by the Auger recombination process in charged QDs.[39] Thus, the off-state decay rates cannot be used to determine the ET rate and are not further discussed in this paper. Instead, we focus on the distribution and fluctuation of the on-state decay rates.

As shown in Figure 3c1−c4, the on-state decay rates increase in single QD−C60 complexes with higher C60-to-QD ratios. This trend is consistent with the ensemble-averaged fluorescence decay results shown in Figure 1b and suggests increased ET rates from sample 2 to sample 4. Furthermore, the distribution of on-states exciton decay rates in free QDs (Figure 3c1), showing an average intrinsic decay rate k_0 at 0.048 ns^{-1}, is much narrower than those in QD−C60 complexes (Figure 3c2−c4). We assume that ET from QD to C60 adds an additional decay pathway, $k_{ET}(t)$, but does not affect the distribution of intrinsic exciton decay processes (with an average rate k_0) in the QD−C60 complexes. Within this model, the fluctuation of the exciton on-state decay rates in QD−C60 complexes results mainly from the fluctuation of ET rates. Because of the narrow distribution of intrinsic decay rates, ET rate trajectories for QD *i* ($k_{ET,i}(t)$) can be calculated from the exciton decay rate trajectory $k_i(t)$ following eq 1:

$$k_{ET,i}(t) = k_i(t) - k_0 \quad (1)$$

Using eq 1, the total histogram of ET rates for all QD−C60 complexes in each sample can be obtained, as shown in Figure 4a. To quantify the static heterogeneity of ET rates in different QD−C60 complexes, the average ET rate of each single QD, $\langle k_{ET,i} \rangle$, was calculated as the arithmetic mean of ET rates along its trajectory:

$$\langle k_{ET,i} \rangle = \frac{1}{N} \sum_{j=1}^{N} k_{ET,i}(t_j) \quad (2)$$

Here, t_j and N are the *j*th and total number of on-state points, respectively, along the trajectory. The probability distributions of the average ET rates of samples 2−4 are shown in Figure 4b.

In addition to varying average ET rates among different QD−C60 complexes, single QD−C60 complexes also show different degrees of fluctuations of ET rates along their trajectories. To characterize the fluctuation, we calculate the standard deviation (SD) of ET rates for each complex:

$$SD_i = \sqrt{\frac{1}{N} \sum_{j=1}^{N} (k_{ET,i}(t_j) - \langle k_{ET,i} \rangle)^2} \quad (3)$$

Histograms of the SD for the three QD−C60 samples are compared in Figure 4c2−c4. With increasing C60-to-QD ratios, the fluctuations of ET rates become larger. However, the relative standard deviations, defined as the ratio of the SD to the average

ET rate, for these complexes are similar, as shown in Figure S3 (Supporting Information). It suggests that the standard deviation increases linearly with the average ET rate for single QD−C60 complexes. To further quantify this linear relationship, we also plot the SD as a function of the average ET for all single QDs. As shown in Figure 4d, linear fits to these plots reveal approximately equal slopes of 0.26, 0.26, and 0.24 for samples, 2, 3, and 4, respectively.

Model for Poisson-Distributed ET Dynamics in Single QD−C60 Complexes. As shown in Figure 4b,c, the histograms of the averages and standard deviations of ET rates for single QD−C60 complexes show Poisson-like distributions, and these quantities are positively correlated. This suggests that the heterogeneities in both the average and the standard deviation are caused by a common underlying distribution. In the following, we propose a model to describe the observed distributions. In this model, we assume that these distributions result mainly from the distribution of the number of adsorbates on each QD within that sample. The QD−C60 complexes are formed by self-assembly, which leads to a distribution of the number of C60s on QDs. Each C60 has only two closely spaced COOH groups (see Figure 1a, inset) and can only bind to one QD, but each QD, with its larger surface area, can accommodate more than one C60. If the adsorption process can be assumed to be random, then the number (n) of adsorbates per QD obeys a Poisson distribution:[17,33,34]

$$p(n;m) = \frac{m^n e^{-m}}{n!} \tag{4}$$

Here, $p(n;m)$ is the probability of finding QDs with n adsorbates and m is the average number of adsorbates per QD for the sample. Let k_1 and SD_1 denote the average and standard deviation of ET rates in the 1:1 C60−QD complexes. It is further assumed that, in the n:1 C60−QD complex, the n C60 molecules act as n independent electron acceptors. As a result, the average, k_n, and standard deviation, SD_n, of ET rates in the n:1 C60−QD complex are given by

$$k_n = nk_1 \tag{5}$$

$$SD_n = nSD_1 \tag{6}$$

In a sample with an average C60-to-QD ratio of m, the probability distribution of average ET rates and standard deviations in QD−C60 complexes is given by

$$p(m;k_n) = \frac{m\left(\frac{k_n}{k_1}\right)e^{-m}}{\left(\frac{k_n}{k_1}\right)!} \tag{7}$$

$$p(m;SD_n) = \frac{m\left(\frac{SD_n}{SD_1}\right)e^{-m}}{\left(\frac{SD_n}{SD_1}\right)!} \tag{8}$$

Within this model, the dynamic fluctuation of ET rates for the n:1 complexes should lead to a Gaussian distribution of ET rates with a center at nk_1 and width of nSD_1. Furthermore, there is a distribution of the number of C60 molecules on the QDs in the ensemble of self-assembled single QD−C60 complexes. Accounting for both effects, the total distribution of the ET rate in each sample of single QD−C60 complexes can be written as

$$p(k_{ET}) = \sum_{n=1}^{\infty} \frac{m^n e^{-m}}{n!} \cdot \frac{1}{\sqrt{2\pi}(n \cdot SD_1)} e^{-\frac{(k_{ET} - nk_1)^2}{2(n \cdot SD_1)^2}} + e^{-m}\delta(k_{ET}) \tag{9}$$

where the last term represents the contribution of free QDs in the ensemble.

The distributions shown in Figure 4a−c can be fitted according to eqs 9, 7, and 8, respectively. For each sample, the same value of m is used to fit the total distribution of ET rates and the distributions of the average and standard deviations of ET rates. Furthermore, for samples of different ratios, the same k_1 and SD_1 values are used, whereas the m values are allowed to change. Because of the linear relationship between k_1 and SD_1 (shown in Figure 4d), we have restrained the value of SD_1 to be $0.25k_1$. In the fitting process, the histograms of the total ET rate distribution (Figure 4a) were first fitted to obtain the value for k_1 (and SD_1) and three m values (one for each sample). The histograms in Figure 4b,c were then binned according to the values of k_1 and SD_1 and fitted using the same sets of four fitting parameters. This process is repeated until the best fits for all nine sets of distributions (panels a1−c3) are obtained. These parameters, m, k_1, and SD_1, obtained from the best fits (shown in Figure 4) are listed in Table 1. From the fitting parameter k_1 (SD_1), we can also calculate the number of adsorbates, n, for each average ET rate (standard deviation) according to eq 5 (6), which is also labeled in Figure 4b (c).

TABLE 1. Fitting Parameters for the Distributions of the Averages and Standard Deviations of ET Rates in Single QD−C60 Complexes[a,b]

single QD−C60 fluorescence decay				ensemble-averaged fluorescence decay	
k_1 (ns^{-1})[a]	SD_1 (ns^{-1})[a]	sample no.	m[b]	sample no.	m[b]
0.10	0.025	2	0.3	B	0.3
		3	1.8	C	1.2
		4	6	D	2.2

[a] k_1 and SD_1 are the average and standard deviation, respectively, of ET rates in 1:1 C60-to-QD complexes. [b] m is the average C60-to-QD ratio of the sample.

The parameters obtained from the single QD measurement should also be able to describe the ensemble-averaged fluorescence decay curves shown in Figure 2. The ensemble-averaged fluorescence decay can be described by the following expression

$$[N(t)] = [N(0)]\left[\int_0^\infty p(k_{ET})e^{-k_{ET}t}dk_{ET}\right]\cdot f_{Free}(t) \qquad (10)$$

where $[N(t)]$ and $[N(0)]$ are the population of excited QDs at time t and 0, respectively. $f_{Free}(t)$ is the fluorescence decay of free QDs, which can be independently measured and fitted. The values of k_1 and SD_1 were determined from fitting the data for single QD−C60 complexes, leaving only the average C60-to-QD ratio m as a fitting parameter. As shown in Figure 1b, the ensemble-averaged fluorescence decay curves for ratios B, C, and D can be well fitted to this model. The average ratios obtained from the fits are 0.3, 1.2, and 2.2, respectively, as shown in Table 1. These values agree with the trend of C60 absorption in the UV−visible spectra (Figure 1a) of these samples. Unfortunately, a quantitative comparison is not possible because the exact ratios of C60 to QD are not known in these samples due to the non-negligible solubility of modified C60 molecules in water.

As shown in Figure 4a−c, the proposed model under-represents the distributions at high ET rates and standard deviations. This may be caused by the contributions of off-states in these regions. It has been proposed previously that there exist various charged QD states with a continuous distribution of emission levels and lifetimes.[59,65] Furthermore, charge separation in the QD−C60 complexes generates a positively charged QD and a reduced C60. The QD exciton lifetime in this charge-separated state has not been measured. We have also assumed Gaussian distributions of the fluctuations of ET rates for the single QD−C60 complexes in eq 9, which do not accurately describe a small tail at the high ET rate region in the histograms of single QD−C60 complexes (see Figure 3b). Nevertheless, it appears that the proposed model can adequately describe the overall distributions of the averages and standard deviations of ET rates in single QD−C60 complexes, the ensemble-averaged fluorescence decay kinetics, and their dependences on the C60-to-QD ratio. It suggests that the most dominating heterogeneity in self-assembled QD heterostructures, such as the QD−C60 complexes, is caused by the Poisson distribution of the number of partners on the QD. This implies that other heterogeneities, such as the distribution of QD sizes, appear to be much smaller in comparison. The proposed model assumes a random adsorption process, which should be obeyed when the interaction between the adsorbates is negligible or is much smaller than the adsorbate−QD interaction. Under these conditions, it is also reasonable to assume that these adsorbates act as independent electron acceptors, which leads to the observed correlated Poisson distributions of the standard deviations and averages of ET rates. We believe that these assumptions are likely valid for many other self-assembled QD nanostructures and the averages and dynamical fluctuation (measured by standard deviations) of their properties (such as electron- and energy-transfer rates) may also follow the correlated Poisson distributions reported here for the QD−C60 complexes.

Our result shows that, in addition to the heterogeneity caused by the statistical distribution of the number of adsorbates in the QD−C60 complexes, there are significant dynamic fluctuations of ET rates in the 1:1 complexes. Unfortunately, the current experiment does not directly probe the origin of the fluctuation. According to the Marcus theory of nonadiabatic electron transfer, it can originate from the dynamic variation of reorganization energy, free energy change, and/or electronic coupling strength for electron transfer.[68] Among these parameters, a change of electronic coupling strength is most likely because of the possibility of many C60-QD adsorption conformations. In a previous study of single molecule electron transfer from molecular sensitizers to TiO_2, we show that the presence of adsorbate conformations at the interface is responsible for the dynamical fluctuation of ET rates on the single molecule level.[69] It is likely that these dynamic fluctuations are another common feature for many interfacial ET processes in nanostructures.[14,70]

In conclusion, the electron-transfer dynamics in self-assembled QD−C60 complexes were studied by single QD fluorescence spectroscopy and ensemble-averaged transient absorption and fluorescence decay measurements. Both the single QD and the ensemble-averaged measurements show that the exciton quenching rate increases with the C60-to-QD ratio and can be attributed to the increasing electron-transfer rates from the QD to C60 in these samples. Comparison with the fluorescence decay trajectories of free QDs show that the ET rates of single QD−C60 complexes exhibit large fluctuation with time. Furthermore, the amplitude of the fluctuation (as measured by the standard deviation) increases linearly with the average ET rate, and both obey Poisson statistics. This finding suggests that the distributions in these quantities are caused by a common heterogeneity in the sample. We propose a model that assumes a random adsorption process for C60 molecules on QDs and that the adsorbates act as independent electron acceptors. According to this model, both the averages and the standard deviations of ET rates obey Poisson distributions, caused by the Poisson distribution of

the number of adsorbates on the QDs. This model was shown to satisfactorily describe the measured distributions of ET rates, average ET rates, and standard deviations of single QD−C60 complexes, as well as the ensemble-averaged fluorescence decay kinetics. Our findings suggest that, in many self-assembled QD nanostructures, such as the QD−C60 complexes, there is a statistical distribution of the number of adsorbed partners on the QDs and this leads to distributions of the averages and standard deviation of their interfacial dynamic properties.

METHODS

Sample Preparation. Water-soluble CdSe/$CdS_{2\ ML}$/$CdZnS_{1\ ML}$/$ZnS_{1\ ML}$ core/shell QDs with the first exciton peak at 585 nm were obtained from Ocean NanoTech, LLC, USA. The monomalonic derivative of fullerene C60 was prepared by the Bingel cyclopropanation[71,72] reaction as previously detailed.[73] The QD−C60 complexes were prepared by adding C60 powder into QD water solutions, followed by sonication of the mixture and filtration to remove undissolved C60. The C60-to-QD ratio was controlled by the sonication time. For the ensemble-averaged measurement, samples B, C, and D were prepared with the same QD concentration (~μM) and different sonication times (2, 4, and 6 h, respectively). A free QD sample (A) of the same concentration was also prepared for the comparison. Four samples (1−4) of increasing C60-to-QD ratio were also prepared in similar ways for single QD measurements, although the concentration of QDs is much lower (10 pM). Sample 1 is free QDs, and samples 2, 3, and 4 were prepared with sonication times of 10, 30, and 60 min, respectively. For both single QD and ensemble-averaged fluorescence measurements, the solutions were spin-coated on thin glass coverslips and dried in air.

Single and Ensemble-Averaged QD Fluorescence Decay. The single QD fluorescence decay was measured using a home-built scanning confocal microscope. Femtosecond laser pulses (~100 fs) with a repetition rate of 80 MHz were generated with a mode-locked Ti:Sapphire laser (Tsunami oscillator pumped by a 10 W Millennia Pro, Spectra-Physics). The output centered at 1000 nm was passed through a pulse picker (Conoptics, USA) to reduce the repetition rate by a factor of 9. Excitation pulses at 500 nm were generated by second-harmonic generation of the 1000 nm pulses in a BBO crystal. The excitation beam (~200 nW) was focused through an objective (100× N.A 1.4, oil immersion, Olympus) down to a diffraction-limited spot on the sample, which was spin-coated onto glass coverslips and placed on a piezo scanner (Mad City Laboratories). The resulting epi-fluorescence from the sample was detected by an avalanche photodiode (APD, PerkinElmer SPCM-AQR-14). The APD output was analyzed by a time-correlated single photon counting (TCSPC) board (Becker & Hickl, SPC 600). The instrument response function for the fluorescence lifetime measurement had a full width at half-maximum of ~500 ps. The ensemble-averaged fluorescence decays were measured in the same setup with samples that were prepared with much higher concentrations of QD−C60 complexes.

Acknowledgment. The work was supported by the National Science Foundation (CHE-0848556 to T.L. and CHE-0951743 to W.Z.) and the Petroleum Research Fund (PRF no. 49286-ND6 to T.L.).

Supporting Information Available: Ensemble-averaged transient absorption spectra and kinetics and relative standard deviations of ET rates in single QD−C60 complexes. This material is available free of charge *via* the Internet at http://pubs.acs.org.

REFERENCES AND NOTES

1. Huynh, W. U.; Dittmer, J. J.; Alivisatos, A. P. Hybrid Nanorod-Polymer Solar Cells. *Science* **2002**, *295*, 2425–2427.
2. Robel, I.; Subramanian, V.; Kuno, M.; Kamat, P. V. Quantum Dot Solar Cells. Harvesting Light Energy with CdSe Nanocrystals Molecularly Linked to Mesoscopic TiO_2 Films. *J. Am. Chem. Soc.* **2006**, *128*, 2385–2393.
3. Tachibana, Y.; Akiyama, H. Y.; Ohtsuka, Y.; Torimoto, T.; Kuwabata, S. CdS Quantum Dots Sensitized TiO_2 Sandwich Type Photoelectrochemical Solar Cells. *Chem. Lett.* **2007**, *36*, 88–89.
4. Achermann, M.; Petruska, M. A.; Koleske, D. D.; Crawford, M. H.; Klimov, V. I. Nanocrystal-Based Light-Emitting Diodes Utilizing High-Efficiency Nonradiative Energy Transfer for Color Conversion. *Nano Lett.* **2006**, *6*, 1396–1400.
5. Steckel, J. S.; Snee, P.; Coe-Sullivan, S.; Zimmer, J. P.; Halpert, J. E.; Anikeeva, P.; Kim, L.-A.; Bulovic, V.; Bawendi, M. G. Color-Saturated Green-Emitting QD-LEDS. *Angew. Chem., Int. Ed.* **2006**, *45*, 5796–5799.
6. Colvin, V. L.; Schlamp, M. C.; Alivisatos, A. P. Light-Emitting Diodes Made from Cadmium Selenide Nanocrystals and a Semiconducting Polymer. *Nature* **1994**, *370*, 354–357.
7. Bruchez, M.; Moronne, M.; Gin, P.; Weiss, S.; Alivisatos, A. P. Semiconductor Nanocrystals as Fluorescent Biological Labels. *Science* **1998**, *281*, 2013–2016.
8. Chan, W. C. W.; Nie, S. Quantum Dot Bioconjugates for Ultrasensitive Nonisotopic Detection. *Science* **1998**, *281*, 2016–2018.
9. Medintz, I. L.; Clapp, A. R.; Brunel, F. M.; Tiefenbrunn, T.; Uydea, H. T.; Chang, E. L.; Deschamps, J. R.; Dawson, P. E.; Mattoussi, H. Proteolytic Activity Monitored by Fluorescence Resonance Energy Transfer through Quantum-Dot-Peptide Conjugates. *Nat. Mater.* **2006**, *5*, 581–589.
10. Funston, A. M.; Jasieniak, J. J.; Mulvaney, P. Complete Quenching of CdSe Nanocrystal Photoluminescence by Single Dye Molecules. *Adv. Mater.* **2008**, *20*, 4274–4280.
11. Curutchet, C.; Franceschetti, A.; Zunger, A.; Scholes, G. D. Examining Forster Energy Transfer for Semiconductor Nanocrystalline Quantum Dot Donors and Acceptors. *J. Phys. Chem. C* **2008**, *112*, 13336–13341.
12. Medintz, I. L.; Mattoussi, H. Quantum Dot-Based Resonance Energy Transfer and Its Growing Application in Biology. *Phys. Chem. Chem. Phys.* **2009**, *11*, 17–45.
13. Dayal, S.; Burda, C. Surface Effects on Quantum Dot-Based Energy Transfer. *J. Am. Chem. Soc.* **2007**, *129*, 7977.
14. Issac, A.; Jin, S.; Lian, T. Intermittent Electron Transfer Activity from Single CdSe/ZnS Quantum Dots. *J. Am. Chem. Soc.* **2008**, *130*, 11280–11281.
15. Boulesbaa, A.; Issac, A.; Stockwell, D.; Huang, Z.; Huang, J.; Guo, J.; Lian, T. Ultrafast Charge Separation at CdS Quantum Dot/Rhodamine B Molecule Interface. *J. Am. Chem. Soc.* **2007**, *129*, 15132–15133.
16. Huang, J.; Stockwell, D.; Huang, Z.; Mohler, D. L.; Lian, T. Photoinduced Ultrafast Electron Transfer from CdSe Quantum Dots to Re-Bipyridyl Complexes. *J. Am. Chem. Soc.* **2008**, *130*, 5632–5633.
17. Huang, J.; Huang, Z.; Jin, S.; Lian, T. Exciton Dissociation in CdSe Quantum Dots by Hole Transfer to Phenothiazine. *J. Phys. Chem. C* **2008**, *112*, 19734–19738.
18. Kamat, P. Quantum Dot Solar Cells. Semiconductor Nanocrystals as Light Harvesters. *J. Phys. Chem. C* **2008**, *112*, 18737–18753.
19. Rossetti, R.; Beck, S. M.; Brus, L. E. Direct Observation of Charge-Transfer Reactions across Semiconductor: Aqueous Solution Interfaces Using Transient Raman Spectroscopy. *J. Am. Chem. Soc.* **1984**, *106*, 980–984.
20. Rossetti, R.; Brus, L. E. Picosecond Resonance Raman Scattering Study of Methylviologen Reduction on the

Surface of Photoexcited Colloidal CdS Crystallites. *J. Phys. Chem.* **1986**, *90*, 558–560.
21. Ramsden, J. J.; Gratzel, M. Formation and Decay of Methylviologen Radical Cation Dimers on the Surface of Colloidal CdS: Separation of Two- and Three-Dimensional Relaxation. *Chem. Phys. Lett.* **1986**, *132*, 269–272.
22. Henglein, A. Catalysis of Photochemical Reactions by Colloidal Semiconductors. *Pure Appl. Chem.* **1984**, *56*, 1215–1224.
23. Logunov, S.; Green, T.; Marguet, S.; El-Sayed, M. A. Interfacial Carriers Dynamics of CdS Nanoparticles. *J. Phys. Chem. A* **1998**, *102*, 5652–5658.
24. Burda, C.; Green, T. C.; Link, S.; El-Sayed, M. A. Electron Shuttling across the Interface of CdSe Nanoparticles Monitored by Femtosecond Laser Spectroscopy. *J. Phys. Chem. B* **1999**, *103*, 1783–1788.
25. Blackburn, J. L.; Ellingson, R. J.; Micic, O. I.; Nozik, A. J. Electron Relaxation in Colloidal InP Quantum Dots with Photogenerated Excitons or Chemically Injected Electrons. *J. Phys. Chem. B* **2003**, *107*, 102–109.
26. Robel, I.; Kuno, M.; Kamat, P. V. Size-Dependent Electron Injection from Excited CdSe Quantum Dots into TiO_2 Nanoparticles. *J. Am. Chem. Soc.* **2007**, *129*, 4136–4137.
27. Spanhel, L.; Weller, H.; Henglein, A. Photochemistry of Semiconductor Colloids. 22. Electron Injection from Illuminated CdS into Attached TiO_2 and ZnO Particles. *J. Am. Chem. Soc.* **1987**, *109*, 6632–6635.
28. Nair, G.; Bawendi, M. G. Carrier Multiplication Yields of CdSe and CdTe Nanocrystals by Transient Photoluminescence Spectroscopy. *Phys. Rev. Lett.* **2007**, *76*, 081304.
29. McGuire, J. A.; Joo, J.; Pietryga, J. M.; Schaller, R. D.; Klimov, V. I. New Aspects of Carrier Multiplication in Semiconductor Nanocrystals. *Acc. Chem. Res.* **2008**, *41*, 1810–1819.
30. Pijpers, J. J. H.; Ulbricht, R.; Tielrooij, K. J.; Osherov, A.; Golan, Y.; Delerue, C.; Allan, G.; Bonn, M. Assessment of Carrier-Multiplication Efficiency in Bulk PbSe and PbS. *Nat. Phys.* **2009**, *5*, 811–814.
31. Beard, M. C.; Midgett, A. G.; Hanna, M. C.; Luther, J. M.; Hughes, B. K.; Nozik, A. J. Comparing Multiple Exciton Generation in Quantum Dots to Impact Ionization in Bulk Semiconductors: Implications for Enhancement of Solar Energy Conversion. *Nano Lett.* **2010**, *10*, 3019–3027.
32. Sudeep, P. K.; Early, K. T.; McCarthy, K. D.; Odoi, M. Y.; Barnes, M. D.; Emrick, T. Monodisperse Oligo(Phenylene Vinylene) Ligands on CdSe Quantum Dots: Synthesis and Polarization Anisotropy Measurements. *J. Am. Chem. Soc.* **2008**, *130*, 2384–2385.
33. Pons, T.; Medintz, I. L.; Wang, X.; English, D. S.; Mattoussi, H. Solution-Phase Single Quantum Dot Fluorescence Resonance Energy Transfer. *J. Am. Chem. Soc.* **2006**, *128*, 15324–15331.
34. Boulesbaa, A.; Huang, Z.; Wu, D.; Lian, T. Competition between Energy and Electron Transfer from CdSe QdS to Adsorbed Rhodamine B. *J. Phys. Chem. C* **2010**, *114*, 962–969.
35. Nirmal, M.; Dabbousi, B. O.; Bawendi, M. G.; Macklin, J. J.; Trautman, J. K.; Harris, T. D.; Brus, L. E. Fluorescence Intermittency in Single Cadmium Selenide Nanocrystals. *Nature* **1996**, *383*, 802–804.
36. Empedocles, S.; Bawendi, M. Spectroscopy of Single CdSe Nanocrystallites. *Acc. Chem. Res.* **1999**, *32*, 389–396.
37. Moerner, W. E.; Barbara, P. F. Single Molecules and Atoms. *Acc. Chem. Res.* **1996**, *29*, 561–562.
38. Tamarat, P.; Maali, A.; Lounis, B.; Orrit, M. Ten Years of Single-Molecule Spectroscopy. *J. Phys. Chem. A* **2000**, *104*, 1–16.
39. Jin, S.; Lian, T. Electron Transfer Dynamics from Single CdSe/ZnS Quantum Dots to TiO_2 Nanoparticles. *Nano Lett.* **2009**, *9*, 2448–2454.
40. Cui, S.-C.; Tachikawa, T.; Fujitsuka, M.; Majima, T. Interfacial Electron Transfer Dynamics in a Single CdTe Quantum Dot-Pyromellitimide Conjugate. *J. Phys. Chem. C* **2008**, *112*, 19625–19634.
41. Brown, P.; Kamat, P. V. Quantum Dot Solar Cells. Electrophoretic Deposition of CdSe/C_{60} Composite Films and Capture of Photogenerated Electrons with nC_{60} Cluster Shell. *J. Am. Chem. Soc.* **2008**, *130*, 8890–8891.
42. Zhang, J. Z.; Geselbracht, M. J.; Ellis, A. B. Binding of Fullerenes to Cadmium-Sulfide and Cadmium Selenide Surfaces, Photoluminescence as a Probe of Strong, Lewis Acidity-Driven, Surface Adduct Formation. *J. Am. Chem. Soc.* **1993**, *115*, 7789–7793.
43. Biebersdorf, A.; Dietmuller, R.; Susha, A. S.; Rogach, A. L.; Poznyak, S. K.; Talapin, D. V.; Weller, H.; Klar, T. A.; Feldmann, J. Semiconductor Nanocrystals Photosensitize C-60 Crystals. *Nano Lett.* **2006**, *6*, 1559–1563.
44. Biebersdorf, A.; Dietmueller, R.; Ohlinger, A.; Klar, T. A.; Feldmann, J.; Talapin, D. V.; Weller, H. Photodoping with CdSe Nanocrystals as a Tool to Probe Trap-State Distributions in C-60 Crystals. *Appl. Phys. B* **2008**, *93*, 239–243.
45. Brus, L. E. A Simple-Model for the Ionization-Potential, Electron-Affinity, and Aqueous Redox Potentials of Small Semiconductor Crystallites. *J. Chem. Phys.* **1983**, *79*, 5566–5571.
46. Brus, L. E. Electron−Electron and Electron−Hole Interactions in Small Semiconductor Crystallites: The Size Dependence of the Lowest Excited Electronic State. *J. Chem. Phys.* **1984**, *80*, 4403–4409.
47. Jin, S.; Song, N.; Lian, T. Suppressed Blinking Dynamics of Single QDs on ITO. *ACS Nano* **2010**, *4*, 1545–1552.
48. Markus, T. Z.; Wu, M.; Wang, L.; Waldeck, D. H.; Oron, D.; Naaman, R. Electronic Structure of CdSe Nanoparticles Adsorbed on Au Electrodes by an Organic Linker: Fermi Level Pinning of the Homo. *J. Phys. Chem. C* **2009**, *113*, 14200–14206.
49. Kucur, E.; Riegler, J.; Urban, G. A.; Nann, T. Determination of Quantum Confinement in CdSe Nanocrystals by Cyclic Voltammetry. *J. Chem. Phys.* **2003**, *119*, 2333–2337.
50. Dubois, D.; Kadish, K. M.; Flanagan, S.; Haufler, R. E.; Chibante, L. P. F.; Wilson, L. J. Spectroelectrochemical Study of the C60 and C70 Fullerenes and Their Mono-, Di-, Tri-, and Tetraanions. *J. Am. Chem. Soc.* **1991**, *113*, 4364–4366.
51. Kira, A.; Umeyama, T.; Matano, Y.; Yoshida, K.; Isoda, S.; Park, J. K.; Kim, D.; Imahori, H. Supramolecular Donor−Acceptor Heterojunctions by Vectorial Stepwise Assembly of Porphyrins and Coordination-Bonded Fullerene Arrays for Photocurrent Generation. *J. Am. Chem. Soc.* **2009**, *131*, 3198–3200.
52. Klimov, V. I. Spectral and Dynamical Properties of Multiexcitons in Semiconductor Nanocrystals. *Annu. Rev. Phys. Chem.* **2007**, *58*, 635–673.
53. Huang, J.; Huang, Z.; Yang, Y.; Zhu, H.; Lian, T. Multiple Exciton Dissociation in CdSe Quantum Dots by Ultrafast Electron Transfer to Adsorbed Methylene Blue. *J. Am. Chem. Soc.* **2010**, *132*, 4858–4864.
54. Fisher, B. R.; Eisler, H.-J.; Stott, N. E.; Bawendi, M. G. Emission Intensity Dependence and Single-Exponential Behavior in Single Colloidal Quantum Dot Fluorescence Lifetimes. *J. Phys. Chem. B* **2004**, *108*, 143–148.
55. Efros, A. L.; Rosen, M. Random Telegraph Signal in the Photoluminescence Intensity of a Single Quantum Dot. *Phys. Rev. Lett.* **1997**, *78*, 1110–1113.
56. Shimizu, K. T.; Neuhauser, R. G.; Leatherdale, C. A.; Empedocles, S. A.; Woo, W. K.; Bawendi, M. G. Blinking Statistics in Single Semiconductor Nanocrystal Quantum Dots. *Phys. Rev. B* **2001**, *63*, 205316.
57. Kuno, M.; Fromm, D. P.; Johnson, S. T.; Gallagher, A.; Nesbitt, D. J. Modeling Distributed Kinetics in Isolated Semiconductor Quantum Dots. *Phys. Rev. B* **2003**, *67*, 125304.
58. Peterson, J. J.; Nesbitt, D. J. Modified Power Law Behavior in Quantum Dot Blinking: A Novel Role for Bi-Excitons and Auger Ionizatoin. *Nano Lett.* **2009**, *9*, 338–345.
59. Zhang, K.; Chang, H.; Fu, A.; Alivisatos, A. P.; Yang, H. Continuous Distribution of Emission States from Single CdSe/ZnS Quantum Dots. *Nano Lett.* **2006**, *6*, 843–847.

60. Montiel, D.; Yang, H. Observation of Correlated Emission Intensity and Polarization Fluctuations in Single CdSe/ZnS Quantum Dots. *J. Phys. Chem. A* **2008**, *112*, 9352–9355.
61. Pelton, M.; Smith, G.; Scherer, N. F.; Marcus, R. A. Evidence for a Diffusion-Controlled Mechanism for Fluorescence Blinking of Colloidal Quantum Dots. *Proc. Natl. Acad. Sci. U.S.A.* **2007**, *104*, 14249–14254.
62. Tang, J.; Marcus, R. A. Determination of Energetics and Kinetics from Single-Particle Intermittency and Ensemble-Averaged Fluorescence Intensity Decay of Quantum Dots. *J. Chem. Phys.* **2006**, *125*, 044703.
63. Issac, A.; von Borczyskowski, C.; Cichos, F. Correlation between Photoluminescence Intermittency of CdSe Quantum Dots and Self-Trapped States in Dielectric Media. *Phys. Rev. B* **2005**, *71*, 161302.
64. Schlegel, G.; Bohnenberger, J.; Potapova, I.; Mews, A. Fluorescence Decay Time of Single Semiconductor Nanocrystals. *Phys. Rev. Lett.* **2002**, *88*, 137401.
65. Verberk, R.; van Oijen, A. M.; Orrit, M. Simple Model for the Power-Law Blinking of Single Semiconductor Nanocrystals. *Phys. Rev. B* **2002**, *66*, 233202.
66. Krauss, T. D.; O'Brien, S.; Brus, L. E. Charge and Photoionization Properties of Single Semiconductor Nanocrystals. *J. Phys. Chem. B* **2001**, *105*, 1725–1733.
67. Shimizu, K. T.; Woo, W. K.; Fisher, B. R.; Eisler, H. J.; Bawendi, M. G. Surface-Enhanced Emission from Single Semiconductor Nanocrystals. *Phys. Rev. Lett.* **2002**, *89*, 117401.
68. Marcus, R. A.; Sutin, N. Electron Transfers in Chemistry and Biology. *Biochem. Biophys. Acta* **1985**, *811*, 265–322.
69. Jin, S.; Snoeberger, R. C., III; Issac, A.; Stockwell, D.; Batista, V. S.; Lian, T. Single-Molecule Interfacial Electron Transfer in Donor-Bridge-Nanoparticle Acceptor Complexes. *J. Phys. Chem. B* **2010**, *114*, 14309–14319.
70. Biju, V.; Micic, M.; Hu, D.; Lu, H. P. Intermittent Single-Molecule Interfacial Electron Transfer Dynamics. *J. Am. Chem. Soc.* **2004**, *126*, 9374–9381.
71. Bingel, C. Cyclopropylation of Fullerenes. *Chem. Ber.* **1993**, *126*, 1957–1959.
72. Lamparth, I.; Hirsch, A. Water-Soluble Malonic Acid Derivatives of C_{60} with a Defined Three-Dimensional Structure. *J. Chem. Soc., Chem. Commun.* **1994**, 1727–1728.
73. Zhan, W.; Jiang, K. A Modular Photocurrent Generation System Based on Phospholipid-Assembled Fullerenes. *Langmuir* **2008**, *24*, 13258–13261.